NASA
Technical Memorandum 102427

AVSCOM
Technical Report 89-C-021

On the Numerical Solution of the Dynamically Loaded Hydrodynamic Lubrication of the Point Contact Problem

Sang G. Lim
Case Western Reserve University
Cleveland, Ohio

David E. Brewe
Propulsion Directorate
U.S. Army Aviation Research and Technology Activity—AVSCOM
Lewis Research Center
Cleveland, Ohio

and

Joseph M. Prahl
Case Western Reserve University
Cleveland, Ohio

February 1990

NASA

US ARMY
AVIATION
SYSTEMS COMMAND
AVIATION R&T ACTIVITY

ON THE NUMERICAL SOLUTION OF THE DYNAMICALLY LOADED HYDRODYNAMIC LUBRICATION OF THE POINT CONTACT PROBLEM

Sang G. Lim*
Department of Mechanical Engineering
Case Western Reserve University
Cleveland, Ohio 44106

David E. Brewe
Propulsion Directorate
U.S. Aviation Research and Technology Activity - AVSCOM
Lewis Research Center
Cleveland, Ohio 44135

and

Joseph M. Prahl
Department of Mechanical Engineering
Case Western Reserve University
Cleveland, Ohio 44106

ABSTRACT

The transient analysis of hydrodynamic lubrication of a point-contact is presented. A body-fitted coordinate system is introduced to transform the physical domain to a rectangular computational domain, enabling the use of the Newton-Raphson method for determining pressures and locating the cavitation boundary, where the Reynolds boundary condition is specified. In order to obtain the transient solution, an explicit Euler method is used to effect a time march. The transient dynamic load is a sinusoidal function of time with frequency, fractional loading, and mean load as parameters.

Results include the variation of the minimum film thickness and phase-lag with time as functions of excitation frequency. The results are compared with the analytic solution to the transient step bearing problem with the same dynamic loading function. The similarities of the results suggest an approximate model of the point contact minimum film thickness solution.

E-5193

*NASA Resident Research Associate at Lewis Research Center.

INTRODUCTION

Nonconformal contact machine elements in power train systems such as gears, rolling element bearings, and cam and follower mechanisms are subject to transient lubrication. The transient characteristics are due to the time variation of loading, geometry, and the rolling or sliding speed in the line or point contact. These variations result in a squeeze effect which affects the minimum film thickness distribution. An example of this is the ball bearings in a rotordynamic system in which there exist cyclic variations of the dynamic load. Recently, the transient hydrodynamic and elastohydrodynamic line contact problem has received much attention (Refs. 1 to 3). Among the several authors, Vichard (Ref. 1) pioneered the basic transient characteristics of the line contact problem analytically and experimentally including the viscous damping phenomenon. In this paper, the transient solution of the hydrodynamically lubricated point contact presented.

In solving the point contact transient problem numerically, a fast computer code is needed to solve the two dimensional Reynolds equation for many time steps. Numerical methods for solving the simultaneous equations resulting from the discretization of the Reynolds equation are usually performed using either iterative methods or semidirect methods (Ref. 4). The former commonly involves the Gauss-Seidel method, the latter combines the Newton-Raphson method with a direct inversion of the Jacobian matrix. An important difference between the iterative method and the semidirect method is that the initial guess plays an important role in the latter, whereas the former is relatively insensitive to the initial guess. With the semidirect method, the use of a previous solution as an initial guess accelerates the solution process, but a good initial guess usually does not help the iterative method significantly (Ref. 4). The semidirect method is preferred for transient problem since the solution of the previous time step accelerates the

next step solution. Furthermore, the Newton-Raphson method has a quadratic convergence rate, so, in general, the solution can be terminated within ten iterations. When a parallel processing computer using vectorization is employed the matrix inversion is very fast. In addition, there is no need to use underrelaxation factors, and the solution can be obtained more rigorously than is typical with iterative methods. The matrix inversion can be done by the Thomas algorithm, and there is no need to store the whole Jacobian matrix.

When the semidirect method is used in the point contact problem, the cavitation boundary, where the Reynolds boundary condition (B.C.) is specified, is difficult to locate. There is a fundamental difference between the line contact and the point contact problem. In the line contact case, the Reynolds equation is integrated once; the Neumann condition is introduced; and the integration constant is found as a part of the solution. In the two-dimensional problem, the Reynolds equation can not be integrated. Since the Reynolds B.C. insures mass conservation across the boundary, the cavitation boundary should be located as accurately as possible. However, the location is not known in advance; it is a part of the solution. It is a free boundary where two B.C.'s are present: Dirichlet B.C. (pressure is zero), and Neumann B.C. (normal pressure gradient is zero). The relaxation method of Christopherson (Ref. 5), derived for the hydrodynamic lubrication of a journal bearing, has been used to solve this kind of free boundary value problem. This method truncates negative computed pressures whenever they occur during iteration. However, this method can not be used in the semidirect method. In this work a body-fitted coordinate system is introduced which transforms the unknown boundary into a fixed boundary and the unknown boundary function is introduced into the equations of motion. The smooth cavitation boundary is found up to truncation and machine errors, whereas the result for Christopherson's method is dependent upon the mesh size near the boundary. To

detect the minute change of the cavitation boundary between the adjacent time steps, the current method is desirable. Another advantage of this method is that a nonzero pressure gradient condition can be implemented for very lightly loaded cases where surface tension may play an important role, or for non-Newtonian, viscoelastic fluids.

In the present paper the transient hydrodynamic lubrication of a step bearing is solved analytically to provide physical insight into the transient characteristics of hydrodynamic lubrication. Next, the point contact problem is solved numerically by the Newton-Raphson method with Thomas algorithm. This method is fast and does not require vast computer storage. Parallel processing by vectorization is also utilized.

The variation with time over a loading cycle of the minimum film thickness, squeeze velocity, and the cavitation boundary is studied for a wide range of excitation frequencies.

NOMENCLATURE

F	dimensionless load
F_0	dimenslonless mean load
$\vec{F}$	right hand side equation of discretized equation
f	load, N (point contact), N/m (step bearing)
f_0	mean load, N (point contact), N/m (step bearing)
G	dimensionless cavitation boundary function
G'	first derivative of G with respect to Y
G''	second derivative of G with respect to Y
g	cavitation boundary curve function
H	dimensionless film thickness
H_0	dimensionless minimum film thickness
$\bar{H}_0$	normalized dimensionless minimum film thickness, H_0/H_{0m}

H_{0m}	dimensionless minimum film thickness for F_0
h	film thickness, m
h_0	minimum film thickness, m
k	number of iteration of Newton-Raphson method
L	length of the step bearing, m
ℓ	reference length for order-of-magnitude analysis, m
NI	number of grid in ξ direction
NJ	number of grid in η direction
$\vec{n}$	normal direction vector
P	dimensionless pressure
p	pressure, N/m^2
R	radius of sphere, m
$\vec{R}$	residual vector of discretized equation
t	time, sec
$\vec{u}$	solution vector of the discretized equations
u_m	average surface velocity in x-direction, m/sec
u_0	reference velocity for order-of-magnitude-analysis, m/sec
X	dimensionless coordinate along rolling direction
X_A	dimensionless inlet boundary location in X-direction
x	coordinate along rolling direction
x_A	inlet boundary location in x-direction
Y	dimensionless coordinate transverse to rolling direction
Y_B	dimensionless inlet boundary location in Y-direction
y	coordinate transverse to rolling direction
y_B	inlet boundary location in y-direction
α	viscosity-pressure coefficient, m^2/N
$\bar{\alpha}$	dimensionless viscosity-pressure coefficient

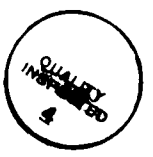

β fractional loading amplitude for sinusoidal loading

γ dimensionless frequency

δ dimensionless film thickness of the step bearing

$\bar{\delta}$ normalized film thickness of step bearing, δ/δ_{0m}

δ_{0m} dimensionless film thickness of the step bearing for mean load

μ lubricant viscosity, Pa·sec

$\bar{\mu}$ dimensionless lubricant viscosity

μ_0 lubricant viscosity at atmospheric pressure, Pa·sec

ν kinematic viscosity, m^2/sec

ξ,η coordinates of transformed domain

ρ lubricant density, kg/m^3

τ dimensionless time

ϕ_s phase angle of the step bearing solution, deg

ϕ_p phase angle of the point contact solution, deg

Ω physical domain

Ω' computational domain

ω frequency of sinusoidal loading, (cycle)/sec

ANALYTICAL SOLUTION OF A STEP BEARING

Consider the simple step bearing shown in Fig. 1. Note that the step bearing used here is subjected to an oscillating normal motion and is closed at the exit end. To the authors' knowledge, this particular solution is not available in the literature and is therefore presented here. The film profile and the dynamic force are:

$$h(x,t) = h(t), \qquad 0 \leq X < L,$$

$$= 0, \qquad x = L, \tag{1}$$

$$f(t) = f_0(1 + \beta \sin \omega t). \tag{2}$$

For an incompressible, isoviscous, Newtonian fluid, the governing equation is,

$$\frac{\partial}{\partial x}\left(h^3 \frac{\partial p}{\partial x}\right) = 12\mu_0 u_m \frac{\partial h}{\partial x} + 12\mu_0 \frac{\partial h}{\partial \tau}\ ; \qquad u_m = \frac{u_1}{2}. \tag{3}$$

The boundary conditions and the initial condition are,

$$\left.\begin{aligned} p &= 0 \quad \text{at} \quad x = 0, \\ h &= 0 \quad \text{at} \quad x = L, \\ h &= h_i \quad \text{when} \quad t = 0. \end{aligned}\right\} \tag{4}$$

With the following definitions,

$$\delta = \frac{h}{L}; \qquad \tau = \frac{t u_m}{L}; \qquad X = \frac{x}{L}; \qquad P = \frac{pL}{\mu_0 u_m}; \qquad F = \frac{f}{\mu_0 u_m}; \qquad \gamma = \frac{\omega L}{u_m},$$

the dimensionless equations are,

$$\frac{\partial}{\partial X}\left(\delta^3 \frac{\partial P}{\partial X}\right) = 12 \frac{\partial \delta}{\partial X} + 12 \frac{\partial \delta}{\partial \tau},$$

$$\left.\begin{aligned} \delta(X,\tau) &= \delta(\tau), \qquad 0 \le X < 1, \\ &= 0, \qquad X = 1, \\ P &= 0 \quad \text{at} \quad X = 0, \\ \delta &= \delta_i \quad \text{when} \quad \tau = 0, \end{aligned}\right\} \tag{5}$$

$$F(\tau) = F_0(1 + \beta \sin \gamma\tau). \tag{6}$$

After integrating Eq. (5) three times using,

$$\int_0^1 P\, dX = F(\tau) \tag{7}$$

the following nonlinear first order differential equation results:

$$\frac{2}{\delta^3}\frac{\partial \delta}{\partial \tau} - \frac{3}{\delta^2} = -\frac{1}{2}F(\tau). \tag{8}$$

The solution of Eq. (8) subject to the B.C.'s in Eq. (5) is,

$$\delta(\tau) = \left[\left(\frac{1}{\delta_i^2} - \frac{F_0}{6} + \frac{F_0 \beta\gamma}{2(\gamma^2 + 9)}\right)e^{-3\tau} + \frac{F_0}{6} + \frac{F_0\beta}{2(\gamma^2 + 9)}(3 \sin \gamma\tau - \gamma \cos \gamma\tau)\right]^{-1/2}. \tag{9}$$

After a sufficiently long time ($\tau \to \infty$), the exponential term vanishes to zero, and the time variation of the film thickness becomes,

$$\delta(\tau) = \delta_{0m}\left[1 + \frac{\beta}{\sqrt{1 + \left(\frac{\gamma}{3}\right)^2}} \sin(\gamma\tau - \phi_s)\right]^{-1/2},$$

where

$$\delta_{0m} = \sqrt{\frac{6}{F_0}}, \qquad \phi_s = \tan^{-1}\left(\frac{\gamma}{3}\right). \tag{10}$$

The formula for the squeeze velocity is obtained by differentiating Eq. (10),

$$\frac{\left(\frac{d\delta}{d\tau}\right)}{\delta_{0m}} = \left(-\frac{\gamma}{2}\right) \frac{\beta}{\sqrt{1 + \left(\frac{\gamma}{3}\right)^2}} \cos(\gamma\tau - \phi_s)\left[1 + \frac{\beta}{\sqrt{1 + \left(\frac{\gamma}{3}\right)^2}} \sin(\gamma\tau - \phi_s)\right]^{-3/2}. \tag{11}$$

ANALYTICAL FORMULATION OF THE POINT CONTACT PROBLEM

The physical model is illustrated in Fig. 2. The radius of the sphere is R and the dynamic force is the same as that of the step bearing. The two dimensional, transient, incompressible form of the Reynolds equation for Newtonian flow is,

$$\frac{\partial}{\partial x}\left(\frac{h^3}{\mu}\frac{\partial p}{\partial x}\right) + \frac{\partial}{\partial y}\left(\frac{h^3}{\mu}\frac{\partial p}{\partial y}\right) = 12u_m\frac{\partial h}{\partial x} + 12\frac{\partial h}{\partial t},$$

where

$$\left.\begin{aligned} p &= p(x,y,t) \\ h &= h(x,y,t) \\ \mu &= \mu(x,y,t). \end{aligned}\right\} \tag{12}$$

The parabolic approximation of the film thickness equation of the sphere is:

$$h = h_0 + \frac{1}{2R}(x^2 + y^2). \tag{13}$$

At a given time, the generated pressure distribution is balanced by the dynamic load,

$$f(t) = \int\int_{\Omega} P(x,y,t)\,dx\,dy. \tag{14}$$

The piezoviscous effect is modelled by the Barus relation (16):

$$\mu = \mu_0 e^{\alpha p}. \tag{15}$$

The boundary conditions are:

$$\left.\begin{aligned} p = 0 \quad &\text{at} \quad x = x_A \qquad 0 \le y \le y_B, \\ p = 0 \quad &\text{at} \quad x_A \le x \le g(y_B,t) \qquad y = y_B, \\ p = 0; \quad \frac{\partial p}{\partial \vec{n}} = 0 \quad &\text{at} \quad x = g(y,t) \qquad 0 \le y \le y_B, \\ \frac{\partial p}{\partial y} = 0 \quad &\text{at} \quad X_A \le x \le g(0,t) \qquad y = 0. \end{aligned}\right\} \tag{16}$$

At the cavitation boundary, $x = g(y,t)$, the pressure and the normal pressure gradient are zero (Reynolds B.C.). Using symmetry at $y = 0$, the Neumann B.C. is imposed and only half of the domain is modelled.

With the following definitions,

$$X = \frac{x}{R}; \qquad Y = \frac{y}{R}; \qquad H = \frac{h}{R}; \qquad P = \frac{pR}{\mu_0 \mu_m}; \qquad F = \frac{f}{\mu_0 u_m R};$$

$$\tau = \frac{u_m t}{R}; \qquad \gamma = \frac{\omega R}{u_m}; \qquad \bar{\mu} = \frac{\mu}{\mu_0}; \qquad G = \frac{g}{R}.$$

the dimensionless equations are:

$$\left.\begin{aligned} &\frac{\partial}{\partial X}\left(\frac{H^3}{\bar{\mu}}\frac{\partial P}{\partial X}\right) + \frac{\partial}{\partial Y}\left(\frac{H^3}{\bar{\mu}}\frac{\partial P}{\partial Y}\right) = 12\,\frac{\partial H}{\partial X} + 12\,\frac{\partial H}{\partial \tau}, \\ &H = H_0 + \frac{1}{2}(X^2 + Y^2), \\ &F(\tau) = 2\int_0^{Y_B}\int_{X_A}^{G(Y)} P(X,Y,\tau)\,dX\,dY, \\ &F(\tau) = F_0(1 + \beta \sin \gamma \tau), \\ &\bar{\mu} = e^{\bar{\alpha}P} \end{aligned}\right\} \tag{17}$$

with $\bar{\alpha} = 1.5131 \times 10^{-8}$ in this study.

To fix the unknown cavitation boundary, the following body-fitted coordinate transformation shown in Fig. 3 is introduced:

$$\xi = \frac{Y_B(X - X_A)}{G(Y,\tau) - X_A},$$

$$\eta = Y, \tag{18}$$

$$|J| = (G(Y,\tau) - X_A)/Y_B.$$

$|J|$ is the Jacobian of the coordinate transformation which shows that as long as $G(Y,\tau)$ is not equal to X_A, there exists a conformal mapping between the physical domain and the computational domain.

The differentiations transforms to the following:

$$\frac{\partial}{\partial X} = \frac{Y_B}{G - X_A}\frac{\partial}{\partial \xi},$$

$$\frac{\partial}{\partial Y} = \frac{\partial}{\partial \eta} - \frac{\xi G'}{G - X_A}\frac{\partial}{\partial \xi},$$

$$\frac{\partial^2}{\partial X^2} = \frac{Y_B^2}{(G - X_A)^2}\frac{\partial^2}{\partial \xi^2},$$

$$\frac{\partial^2}{\partial Y^2} = \frac{\xi^2 (G')^2}{(G - X_A)^2}\frac{\partial^2}{\partial \xi^2} - \frac{2\xi G'}{G - X_A}\frac{\partial^2}{\partial \xi \partial \eta} + \frac{\partial^2}{\partial \eta^2} + \frac{\xi\left[2(G')^2 - G''(G-X_A)\right]}{(G - X_A)^2}\frac{\partial}{\partial \xi}. \tag{19}$$

The Reynolds equation in the (ξ,η) system is,

$$AP_{\xi\xi} + BP_{\xi\eta} + CP_{\eta\eta} + DP_{\xi} + EP_{\eta} + F = 0, \tag{20}$$

where

$$A = A_3\left[Y_B^2 + \xi^2 (G')^2\right],$$

$$B = A_3[-2\xi G'(G-X_A)],$$

$$C = A_3(G - X_A)^2,$$

$$D = A_1 Y_B(G - X_A) - A_2 \xi G'(G - X_A) + A_3 \xi\left[2(G')^2 - G''(G - X_A)\right],$$

$$E = A_2(G - X_A)^2,$$

$$F = -A_4(G - X_A)^2,$$

$$A_1 = \frac{3H^2}{\bar{\mu}} \frac{\partial H}{\partial X} + H^3 \frac{\partial}{\partial X}\left(\frac{1}{\bar{\mu}}\right),$$

$$A_2 = \frac{3H^2}{\bar{\mu}} \frac{\partial H}{\partial Y} + H^3 \frac{\partial}{\partial Y}\left(\frac{1}{\bar{\mu}}\right),$$

$$A_3 = \frac{H^3}{\bar{\mu}},$$

$$A_4 = 12 \frac{\partial H}{\partial X} + 12 \frac{\partial H}{\partial \tau}.$$

In the above formulation, A_1, A_2, A_3, and A_4 can be transformed to the (ξ,η) coordinate system using Eq. (19). At the cavitation boundary,

$$\frac{\partial P}{\partial \vec{n}} = \frac{1}{\sqrt{1 + (G')^2}} \left[\frac{1}{G - X_A}(Y_B + \xi(G')^2)\frac{\partial P}{\partial \xi} - G'\frac{\partial P}{\partial \eta}\right] = 0. \tag{21}$$

Since $\partial P/\partial \eta = 0$ at $\xi = Y_B$,

$$\frac{\partial P}{\partial \xi} = 0, \qquad P = 0 \quad \text{at} \quad \xi = Y_B. \tag{22}$$

At $\eta = 0 (Y = 0)$, the symmetry condition is,

$$\frac{\partial P}{\partial Y} = \frac{\partial P}{\partial \eta} - \frac{\xi G'}{G - X_A} \frac{\partial P}{\partial \xi} = 0. \tag{23}$$

But, $G' = 0$ due to the symmetry of cavitation boundary and it follows that,

$$\frac{\partial P}{\partial \eta} = 0 \quad \text{at} \quad \eta = 0. \tag{24}$$

The transformed film thickness equation and the force balance equation are expressed,

$$H(\xi,\eta) = H_0 + \frac{1}{2}\left\{\left[\frac{\xi(G - X_A)}{Y_B} + X_A\right]^2 + \eta^2,\right\} \tag{25}$$

$$F(\tau) = 2\int_0^{Y_B}\int_0^{Y_B} P(\xi,\eta,\tau)\,\frac{(G-X_A)}{Y_B}\,d\xi\,d\eta. \tag{26}$$

In the above formulation, the unknown boundary curve function G is introduced into the governing equations while the computational domain is fixed.

NUMERICAL METHODS

Equation (20) is a nonlinear partial differential equation. The nonlinearity is due to the piezoviscous relation and to the function G in the transformed Reynolds equation.

Spatial Discretization

In order to minimize the number of grid points while maintaining accuracy, a smoothly varying nonuniform spacing is generated by a two-sided stretching function, (hyperbolic tangent) (Ref. 10). The finest spacing is near the cavitation boundary which is also near the maximum pressure gradient.

Figure 4 shows the finite difference mesh structure. The increments in ξ and η and are such that

$$\left.\begin{aligned} \xi_I - \xi_{I-1} &= \Delta\xi \\ \xi_{I+1} - \xi_I &= r_\xi \Delta\xi \\ \eta_J - \eta_{J-1} &= \Delta\eta \\ \eta_{J+1} - \eta_J &= r_\eta \Delta\eta. \end{aligned}\right\} \tag{27}$$

By the Taylor series expansion, the finite difference approximations of derivatives with respect to ξ and η are,

$$\frac{\partial P}{\partial \xi} = \frac{-r_\xi^2 P_{I-1,J} + (r_\xi^2 - 1)P_{I,J} + P_{I+1,J}}{r_\xi(1 + r_\xi)\Delta\xi},$$

$$\frac{\partial P}{\partial \eta} = \frac{-r_\eta^2 P_{I,J-1} + (r_\eta^2 - 1)P_{I,J} + P_{I,J+1}}{r_\eta(1 + r_\eta)\Delta\eta},$$

$$\frac{\partial^2 P}{\partial \xi^2} = 2\,\frac{r_\xi P_{I-1,J} - (r_\xi + 1)P_{I,J} + P_{I+1,J}}{r_\xi(1 + r_\xi)\Delta\xi^2},$$

$$\frac{\partial^2 P}{\partial \eta^2} = 2\,\frac{r_\eta P_{I,J-1} - (r_\eta + 1)P_{I,J} + P_{I,J+1}}{r_\eta(1 + r_\eta)\Delta\eta^2},$$

$$\frac{\partial^2 P}{\partial \xi \partial \eta} = \frac{1}{r_\xi r_\eta(1 + r_\xi)(1 + r_\eta)\Delta\xi\Delta\eta}$$

$$\times \left[r_\xi^2 r_\eta^2 P_{I-1,J-1} - r_\eta^2(r_\xi^2 - 1)P_{I,J-1} - r_\eta^2 P_{I+1,J-1} - r_\xi^2(r_\eta^2 - 1)P_{I-1,J} + (r_\xi^2 - 1)\right.$$

$$\left.\times\,(r_\eta^2 - 1)P_{I,J} + (r_\eta^2 - 1)P_{I+1,J} - r_\xi^2 P_{I-1,J+1} + (r_\xi^2 - 1)P_{I,J+1} + P_{I+1,J+1}\right]. \tag{28}$$

Substituting Eq. (28) into the transformed Reynolds Eq. (20) the following discretized equations results,

$$R_{I,J} = C_1 P_{I-1,J+1} + C_2 P_{I,J+1} + C_3 P_{I+1,J+1} + C_4 P_{I-1,J} + C_5 P_{I,J} + C_6 P_{I+1,J}$$
$$+ C_{7_{I-1,J-1}} + C_8 P_{I,J-1} + C_9 P_{I+1,J-1} + C_{10} = 0, \tag{29}$$

with

$$P_{1,J} = P_{NI,J} = 0 \qquad 1 \le J \le NJ,$$

$$P_{I,NJ} = 0 \qquad 1 \le I \le NI,$$

$$P_{I,0} = P_{I,2} \qquad 1 \le I \le NI,$$

$$P_{NI+1,J} = P_{NI-1,J} \qquad 1 \le J \le NJ.$$

Steady-State Solution Method

The transient solution is formed by computing the steady-state solution for each time step including the squeeze term. The numerical technique for the steady-state solution along with the Thomas algorithm and Newton-Raphson method is described first.

The discretized form of transformed equation is,

$$K(\vec{u})\vec{u} = \vec{F} \tag{30}$$

The vector $\vec{u}$ represents the unknown values, pressures and cavitation boundary. For an isoviscous condition $K(\vec{u})$, contains the function G, and, for a piezoviscous condition, it includes pressures as well. The discretized simultaneous equations are nonlinear. Even for the linear free boundary value problem, it has a nonlinear characteristics since the unknown boundary is associated with the solution.

The Newton-Raphson method is described,

$$\vec{u}_{k+1} = \vec{u}_k - J^{-1}(\vec{u}_k)\vec{R}(\vec{u}_k) \tag{31}$$

where $\vec{R}(\vec{u}_k) = K(\vec{u}_k)\vec{u}_k - \vec{F}$ is the residual vector and $J(\vec{u})$ is the Jacobian of the system of equations. In practice, the iteration is organized as,

$$J(\vec{u}_k)\Delta\vec{u}_k = -\vec{R}(\vec{u}_k), \qquad \vec{u}_{k+1} = \vec{u}_k + \Delta\vec{u}_k. \tag{32}$$

For this study, the vector $\vec{u}$ is,

$$\vec{u} = \left(P_{2,J}, P_{3,J}, \ldots, P_{NI-1,J}, G_J\right)^T, \qquad J = 1, NJ - 1 \tag{33}$$

in which $P_{1,J}$ and $P_{NI,J}$ are zero from the Dirichlet boundary condition. The residual vector $\vec{R}$ is,

$$\vec{R} = \left(R_{2,J}, R_{3,J}, \ldots, R_{NI-1,J}\ R_{NI,J}\right)^T, \qquad J = 1, NJ - 1 \tag{34}$$

The Jacobian matrix is a block tridiagonal matrix in Fig. 5, and each block is a one-sided arrow-shaped matrix, Fig. 6. In the formulation of each block matrix of the Jacobian, the last columns are the differentiations of the residual vector with respect to the cavitation boundary function, G. Since all the coefficients in the discretized Reynolds equation are composed of G_J, G'_J, and G''_J, it is easier to calculate them numerically (Ref. 11) using:

$$\frac{\partial R_{I,J}}{\partial G_J} = \frac{1}{\varepsilon_g}\left[R_{I,J}(G_J + \varepsilon_g, w_{I,J}) - R_{I,J}(G_J, w_{I,J})\right] \tag{35}$$

where $w_{I,J}$ contains all other variables except G_J. The value of ε_g can be chosen to be sufficiently small not only to maintain good accuracy of Eq. (35) but to prevent serious round-off errors. In this calculation, ε_g is set to 10^{-9} in double precision.

The block tridiagonal system of Eq. (30) is solved by the Thomas algorithm (Ref. 12). This algorithm inverts the whole matrix at a time by matrix multiplication and inversion of the block matrix, which is quite fast on a parallel processing computer with small memory storage size equal to 2 x NI x NJ x NJ. The matrix inversion is accomplished using LINPACK.

The Newton-Raphson method requires a good initial guess of the solution. For this purpose, the Gauss-Seidel iteration method is used to get an approximate pressure distribution and cavitation boundary location. Once one solution is obtained by the Newton-Raphson method, it is used for the guess to next solution. The convergence criteria are

(1) pressure

$$\frac{\sum_I \sum_J \left| P^{k+1}_{I\,J} - P^k_{I,J} \right|}{\sum_I \sum_J P^k_{I,J}} < 1.0\times10^{-4}$$

(2) cavitation boundary

$$\frac{\sum_J \left| G_J^{k+1} - G_J^k \right|}{\sum_J G_J^k} < 1.0\times10^{-4}$$

(3) force balance

$$\frac{\left| F_{\text{input}} - F_{\text{output}} \right|}{F_{\text{input}}} < 1.0\times10^{-4}$$

In order to make sure of the convergence, the L_2-norm of the residual vector is monitored. In general, the solution converges within 3 to 8 iterations. In this study, NI = 41, NJ = 31.

Transient Solution Method

For the steady-state solution, the problem is to find H_0 for a given load, or for a hydrodynamic case, the load capacity can be calculated for a given H_0. But, for the transient case, there is an additional unknown value to be determined, the squeeze velocity. The basic solution technique is to use a "time-march." That is, H_0 is fixed from the previous time step, and the squeeze velocity is found that balances the generated pressure distribution with the dynamic force at that time. The detailed computation procedure is provided in Fig. 7. At the first time step, the steady-state Reynolds equation is solved to find H_{0m}, and, fixing H_0, the transient Reynolds equation is solved including the squeeze term to find the squeeze velocity using the force balance equation. For this purpose, a bisection method is used, with an approximate range of squeeze velocities according to the history of dynamic force and the minimum film thickness variation. Once a converged solution is obtained, the minimum film thickness of the next time step is estimated from the following expression:

$$H_0^{n+1} = H_0^n + \left(\frac{\partial H}{\partial \tau}\right)^n \Delta\tau, \quad (n = \text{present time step}) \tag{36}$$

The film thickness and squeeze velocities are established at successive time steps and the calculation is continued beyond the first complete loading cycle until the periodic requirement is reached. The convergence criterion is:

$$\frac{\left|(H_0)_n^{IC+1} - (H_0)_n^{IC}\right|}{(H_0)_n^{IC}} < 1.0\times10^{-4}, \quad IC = \text{number of cycle}$$

In this calculation, 361 time steps with 1° increment are used in one loading cycle.

RESULTS AND DISCUSSION

The analytical solution of the step bearing demonstrates that $\bar{\delta}$ approaches one with a phase-lag of 90° as γ increases (Fig. 8). This asymptotic behavior is due to the squeeze action caused by the dynamic forces. Figure 9 shows the squeeze variation of Eq. (11). This phenomenon is physically similar to a nonlinear massless spring-damper system with forced vibration shown in Fig. 10, sometimes referred as a "half a degree of freedom system." The response of this system is that the amplitude approaches a constant value and the phase-lag goes to 90°. Although the transient solution of the point contact problem can not be solved analytically and requires numerical computation, it may be speculated that basically it also has a similar nonlinear spring-damper system. In the following example, the numerical results of the point contact problem are compared to the step bearing solution.

For this study, $F_0 = 3000$ and $\beta = 0.3$ with different γ's. The minimum film thickness for F_0 is 1.2471×10^{-5} for the isoviscous case and 1.3907×10^{-5} for the piezoviscous effect with $X_A = 0.08$, $Y_B = 0.06$. Figure 11 shows the pressure distribution for F_0 and Fig. 12 delineates the detailed

cavitation boundary curve in which the minimum value of G occurs at $Y = 0$ and it increases up to a certain location and then decreases because of the geometry of the sphere.

Figure 13 illustrates the time variation of the normalized minimum film thickness ($\bar{H}_0$) during one loading cycle with 361 time steps. The squeeze velocity distribution is shown in Fig. 14 for different γ's. These results are qualitatively similar to those of the step bearing solution. However, it should be noted that the order of the nondimensional excitation frequencies is different since L is used as a reference length in the step bearing while R is used for the point contact case.

Equation (10) may be put in the following form,

$$\bar{\delta} = \left[\frac{1}{1 + a_s\beta \sin(\gamma\tau - \phi_s)}\right]^{1/2}$$

where

$$a_s = \frac{1}{\sqrt{1 + (\lambda_s\gamma)^2}} \qquad \phi_s = \tan^{-1}(\lambda_s\gamma) \qquad \lambda_s = \frac{1}{3}. \tag{37}$$

The variation of a_s and ϕ_s are plotted in Fig. 15.

For quantitative analysis of the transient point contact problem, the following formula is suggested by Eq. (37),

$$\bar{H}_0 = \left[\frac{1}{1 + a_p\beta \sin(\gamma\tau - \phi_p)}\right]^2 \tag{38}$$

Equation (38) is deduced based on the fact that H_{0m} is inversely proportional to F_0^2 whereas δ_{0m} to $\sqrt{F_0}$. The unknown values in Eq. (38), a_p and ϕ_p, are obtained by a nonlinear least square fit with 361 data point. Figure 16 shows the comparison between the numerical results and the curve fit. The best curve fit can be obtained by letting the numerator of

Eq. (38) be variable, however, it is near 1, for example, 1.005 for $\gamma = 100$, 1.019 for $\gamma = 1000$. The curve fitting results are recorded in Table 1.

Fig. 17 shows the variation of a_p and ϕ_p, qualitatively, similar characteristics to the analytical step bearing solution with different order of magnitude of γ (Fig.15). The value of λ_p is obtained assuming the following relation,

$$\phi_p = \tan^{-1}(\lambda_p \gamma) \tag{39}$$

λ_p is nearly constant over a wide range of γ, approximately 0.0054. If an analytical solution were possible, the a_p would be a function of λ_p. However, since it also would be a function of the geometry associated with the cavitation boundary, no attempt is made to obtain a form similar to Eq. (37). Instead, for design purposes, Eq. (38) can be used along with Table 1.

For the piezoviscous solution, a_p is smaller than that of the isoviscous solution (Fig. 17), but ϕ_p's are virtually the same. The a_p's asymptotically approach those of the isoviscous case. Figure 18 shows this more vividly. Due to the piezoviscous effect, the distribution of $\bar{H}_0$ is more damped with the same phase angle. The λ_p's for the piezoviscous case are nearly constant and equal to the isoviscous case (see Table 1). This implies that λ_p is a characteristic of the transient point contact problem of the current model.

Figure 19 illustrates the location of the outlet boundary at $Y = 0$ normalized by that for the steady-state solution of F_0. For the steady state case, $G(0,\tau)$ approaches the point of contact as the load increases. However, when γ is greater than zero there exists a substantial variation in $G(0,\tau)$ due to the squeeze action. When the squeeze is downward, $G(0,\tau)$ may be stretched outward and vice versa. For example, when $\gamma = 200$, there is a

downward action between a-b and c-d in Fig. 19, and upward action between b and c. These points correspond to those in Fig. 14.

In the foregoing analysis, the Reynolds Eq. (12) neglects the inertia forces. But, as γ increases, the validity of this assumption becomes suspect. This assumption is examined by an order-of-magnitude-analysis of the steady-state Navier-Stokes equation in Ref. (12). When the modified Reynolds number is much less than one,

$$\left(\frac{\rho u_0 \ell}{\mu}\right)\left(\frac{h_0}{\ell}\right)^2 \ll 1 \tag{40}$$

the inertia forces can be neglected. Here, u_0 is a reference velocity, ℓ is a reference length in the x-direction, and h_0 is that in the film thickness direction. Using,

$$U_0 = R\omega; \qquad \gamma = \frac{R\omega}{u_m} \tag{41}$$

the following relation for the validity of the assumption that inertia forces are negligible is,

$$\gamma \ll \frac{1}{H_0 Re}, \qquad H_0 = \frac{h_0}{R}, \qquad Re = \frac{h_0 u_m}{\nu}. \tag{42}$$

For example, if $H_0 = 10^{-5}$, $R = 10^{-2}$ m, $u = 0.1$ m/sec, and $\nu = 10^{-5}$ m^2/sec,

$$\gamma \ll 10^8 \tag{43}$$

Even for $\gamma = 1000$, inertia effects remain negligible.

CONCLUSIONS

The transient solution of the hydrodynamically-lubricated point contact problem including the squeeze effect is obtained numerically using the ball-on-plane model. A new computational algorithm is implemented to deal with the cavitation boundary by the semidirect method with the advantage of

supercomputing. This method provides a faster and more rigorous way to solve the nonconformal contact problem with a Newtonian fluid than the conventional iterative method, and the flexibility to deal with more complex boundary conditions for lightly loaded bearings and more realistic rheological models.

The qualitative and quantitative analysis is compared with the analytical solution of a dynamically loaded step bearing solution using a nonlinear curve fitting method. It is found that there exists a characteristic similarity in the transient responses to a nonlinear massless (i.e., no inertia) spring-damper system, in terms of the variation of the minimum film thickness and phase angle. According to an order of magnitude analysis, it is confirmed that the inertia-forces are negligible for a wide range of practical excitation frequencies.

These results can be applied to the design of moderately loaded ball bearings in rotordynamic systems and can be extended to gear design adding the time variation of the geometry and speed. For highy loaded elliptical contact case, the elastic deformations and ellipticity parameter need to be considered.

REFERENCE

1. Vichard, J.P., "Transient Effects in the Lubrication of Herzian Contacts," J. Mech. Eng. Sci., 13, 3, pp. 173-189, (1971)
2. Lee, R.T., and Hamrock, B.J., "Squeeze and Entraining Motion in Nonconformal Line Contacts. Part 1-Hydrodynamic Lubrication," J. Trib., 111, 1, pp. 1-7, (1989).
3. Bedewi, M.A., Dowson, D., and Taylor, C.M., "Elastohydrodynamic Lubrication of Line Contacts Subjected to Time Dependent Loading with Particular Reference to Roller Bearing and Cams and Followers," Mechanisms and Surface Distress, Butterworth, Stoneham, England, pp. 289-304 (1986).

4. Macarther, J.W., and Patankar, S.V., "Robust Semidirect Finite Differenoe Methods for Solving the Navier-Stokes and Energy Equations," Int. J. Numer. Methods Fluids, 9, pp. 325-340, (1989).

5. Cryer, C. W., "The Method of Christopherson for Solving Free Boundary Problems for Infinite Journal Bearings by Means of Finite Differences," Math. Comput., 25, 115, pp. 435-443, (1971)

6. Pinkus, O., and Sternlicht, B., Theory of Hydrodynamic Lubrication, McGraw Hill, (1961).

7. Cameron, A., The Principles of Lubrication," John Willy and Sons Inc., (1967).

8. Brewe, D.E., Hamrock, B.J., and Taylor, C.M., "Effect of Geometry on Hydrodynamic Film Thickness," J. Lubr. Technol. 101, 2, pp. 231-239, (1979).

9. Dowson, D., and Taylor, C.M., "Cavitation in Bearings Lubricating Films," Annual Review of Fluid Mechanics, 11, pp. 35-66, (1979).

10. Vinokur, M., "On One-Dimensional Stretching Functions for Finite-Difference Calculations--Computational Fluid Dynamics," J. Compt. Phys. 50, pp. 215-234, (1983).

11. Hunt, R., "The Numerical Solution of Elliptic Free Boundary Problems Using Multigrid Techniques," J. Comput. Phys., 65, pp. 448-461, (1986).

12. Shih, T.M., Numerical Heat Transfer, Hemisphere Publishing Co., (1984).

13. Wolowit, J.A., and Anno, J.N., Modern Developments in Lubrication Mechanics, John Wiley & Sons, (1975).

14. Birkhoff, G., and Hays, D.F., "Free Boundaries in Partial Lubrication," J. Math. Phys., 42, pp. 126-138, (1963).

15. Brewe, D.E., and Hamrock, B.J., "Geometry and Starvation Effects in Hydrodynamic Lubrication," NASA TM-82807, 1982.

16. Conte, S.D., and DeBoor, C., Elementary Numerical Analysis, McGraw Hill, (1972).

17. Carrier, G.F., and Pearson, C.E., Partial Differential Equations: Theory and Techniques, Academic Press, (1976).

TABLE 1 - CURVE FITTING RESULTS OF EQ. (38)

	Isoviscous			Piezoviscous		
γ	α_p	ϕ_p	λ_p	α_p	ϕ_p	λ_p
0	0.890	0.0	-------	0.734	0.0	-------
25	.882	7.0	0.00491	.728	7.0	0.00491
50	.859	14.7	.00523	.709	14.7	.00526
100	.781	28.3	.00538	.646	28.4	.00541
150	.687	39.2	.00544	.571	39.2	.00544
200	.599	47.5	.00545	.499	47.4	.00544
250	.523	53.8	.00546	.438	53.7	.00545
300	.461	58.7	.00547	.386	58.5	.00544
350	.409	62.3	.00545	.343	62.3	.00545
400	.368	65.3	.00544	.309	65.2	.00541
500	.303	69.8	.00544	.255	69.8	.00544
750	.210	76.1	.00539	.176	76.1	.00539
1000	.159	79.4	.00536	.134	79.4	.00536

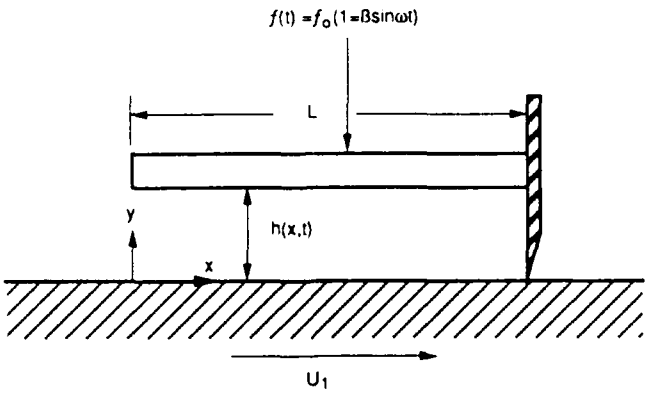

Figure 1. - Schematic view of the step bearing configuration.

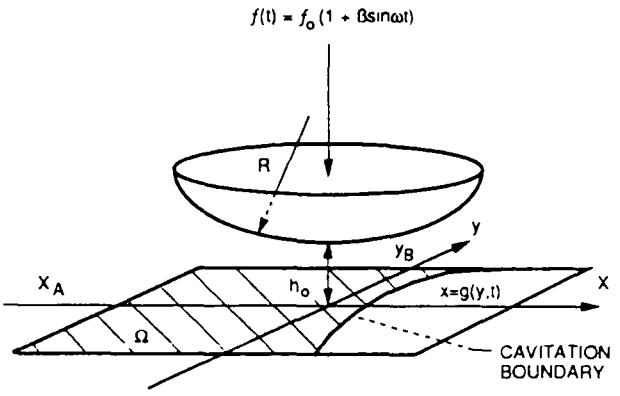

Figure 2. - Physical model of the point contact problem.

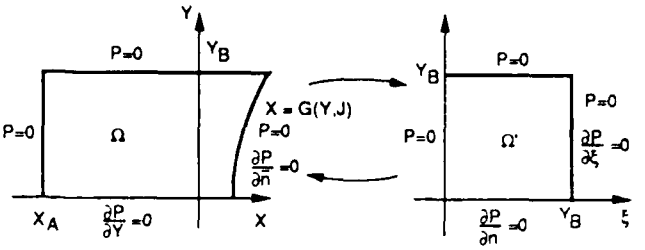

(a) Physical domain. (b) Computational domain.

Figure 3. - Coordinate transformation of the physical domain to the computational domain.

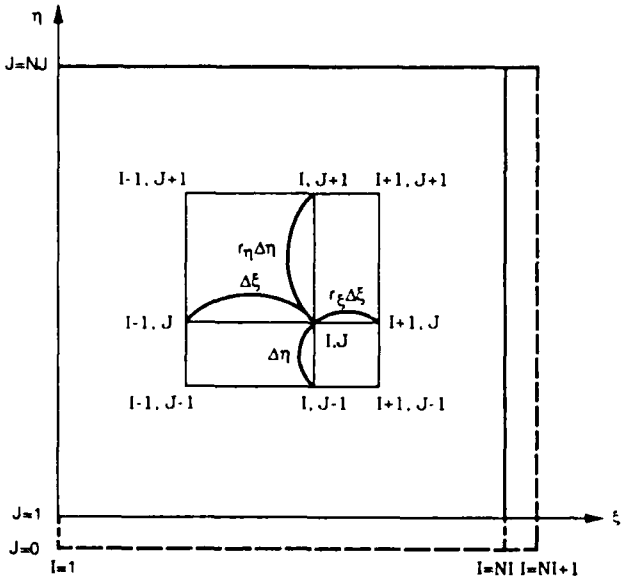

Figure 4. - Finite difference mesh structure.

$$[J] = \begin{bmatrix} [B_1] & [C_1] & & \\ [A_2] & [B_2] & [C_2] & \\ & \ddots & \ddots & \ddots \\ & & [A_{NJ-2}] & [B_{NJ-2}] & [C_{NJ-2}] \\ & & & [A_{NJ-1}] & [B_{NJ-1}] \end{bmatrix}$$

Figure 5. - The Jacobian matrix of eq. [32].

$$[B_J] = \begin{bmatrix} \frac{\partial R_{2,J}}{\partial P_{2,J}} & \frac{\partial R_{2,J}}{\partial P_{2,J}} & & & \frac{\partial R_{2,J}}{\partial P_{2,J}} \\ \frac{\partial R_{2,J}}{\partial P_{2,J}} & \frac{\partial R_{2,J}}{\partial P_{2,J}} & \frac{\partial R_{2,J}}{\partial P_{2,J}} & & \frac{\partial R_{2,J}}{\partial P_{2,J}} \\ & & & & \\ & & \frac{\partial R_{N1-1,J}}{\partial P_{N1-2,J}} & \frac{\partial R_{N1-1,J}}{\partial P_{N1-1,J}} & \frac{\partial R_{N1-1,J}}{\partial G_J} \\ & & & \frac{\partial R_{N1,J}}{\partial P_{N1-1,J}} & \frac{\partial R_{N1-1,J}}{\partial G_J} \end{bmatrix}$$

$J=1, NJ-1$

Figure 6. - The elements in diagonal block matrix.

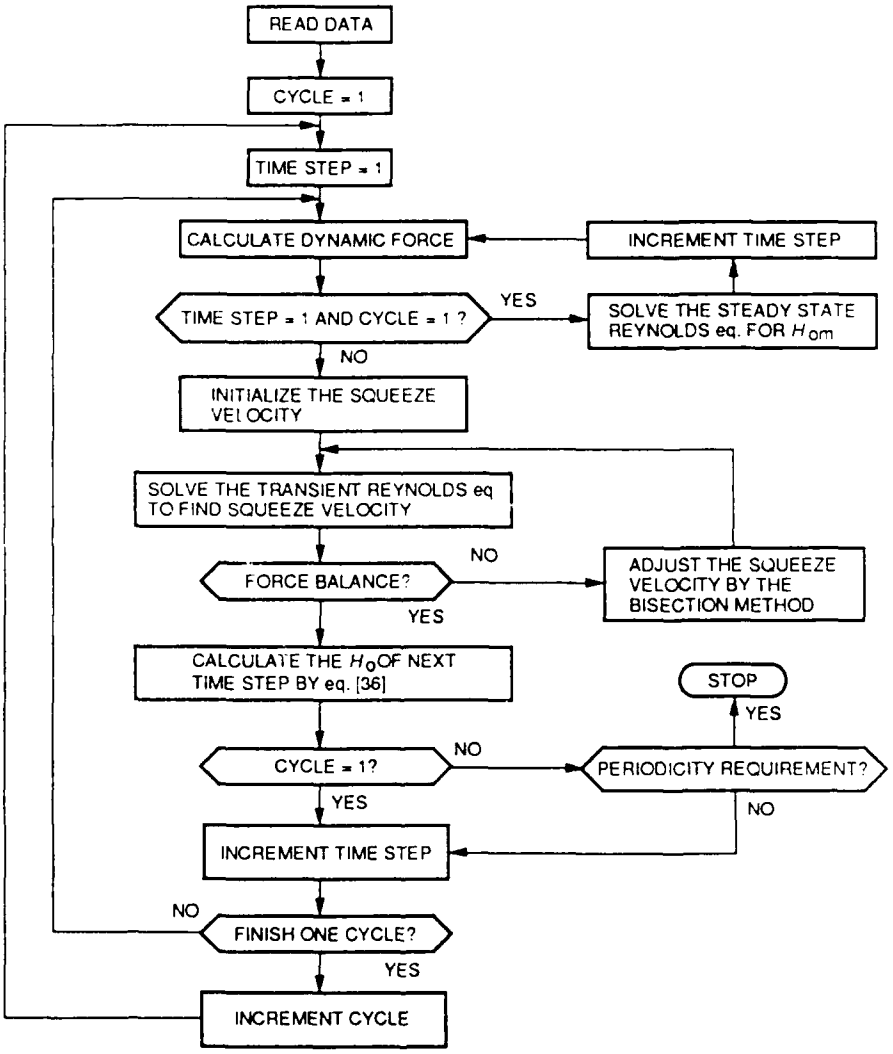

Figure 7. - Flow digram for the transient solution.

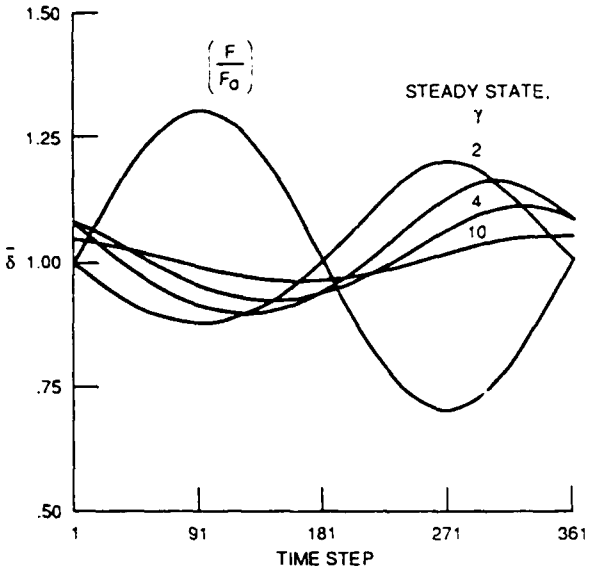

Figure 8. - Normalized film thickness versus nondimensional time during one loading cycle for the step bearing.

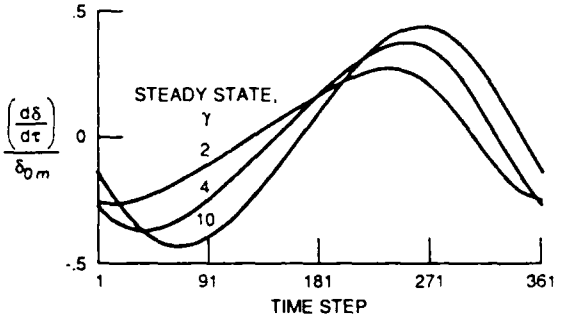

Figure 9 - Squeeze velocity divided by δ_{0m} versus nondimensional time during one loading cycle for the step bearing.

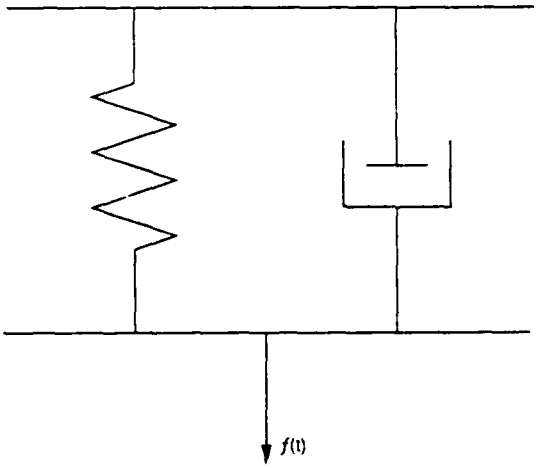

Figure 10. - Half a degree of freedom model.

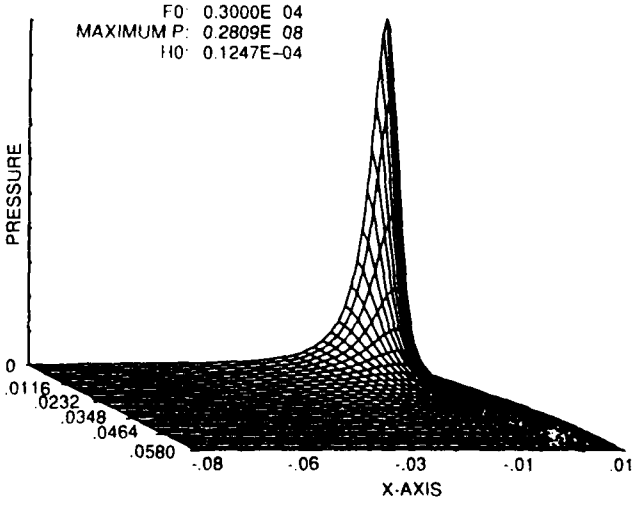

Figure 11. - The pressure distribution of half of the domain for the point contact problem for $F_0 = 3000$.

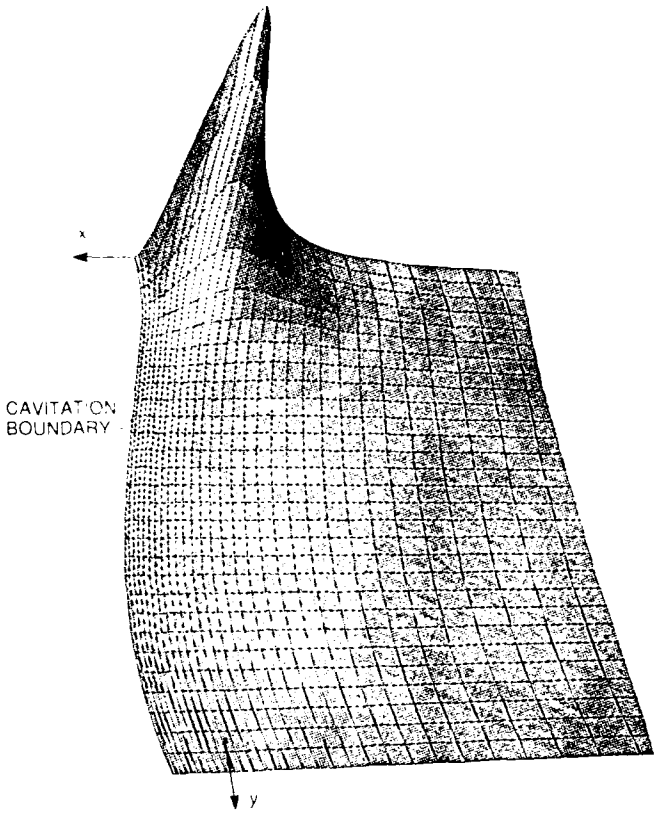

Figure 12. - The detailed pressure distribution of half of the domain near the cavitation boundary curve for the point contact problem.

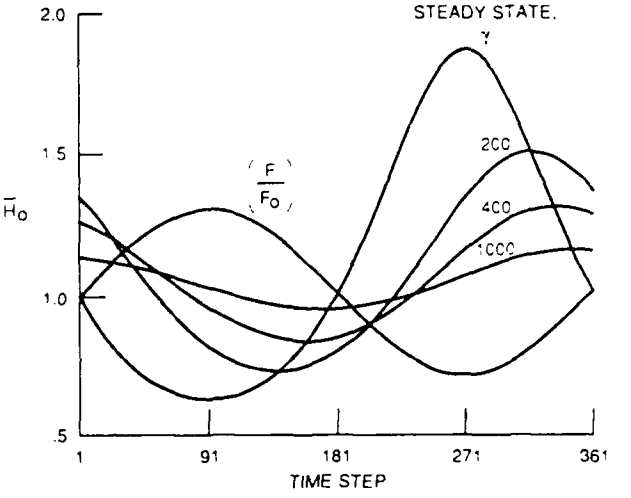

Figure 13. - Normalized minimum film thickness distribution for the point contact problem.

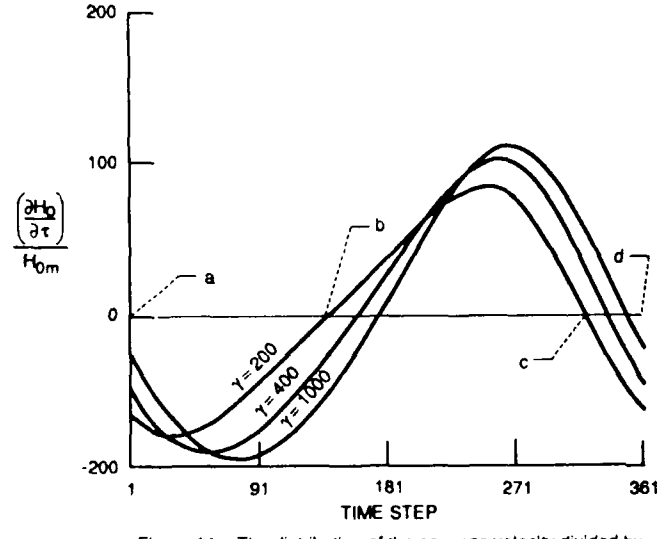

Figure 14. - The distribution of the squeeze velocity divided by the minimum film thickness for the mean load.

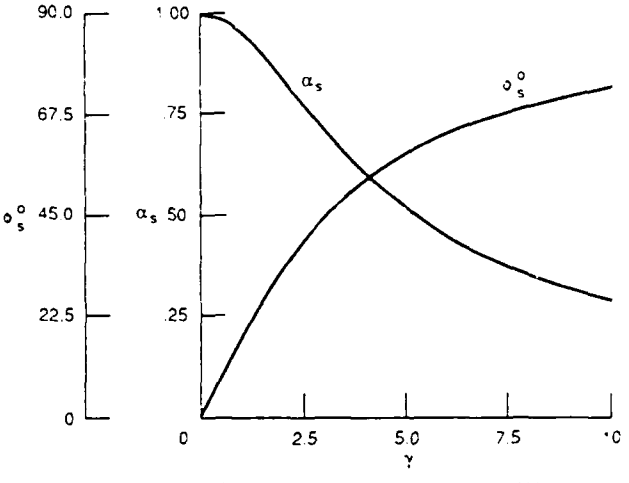

Figure 15. - α_s and ϕ_s as functions of γ, eq. [37].

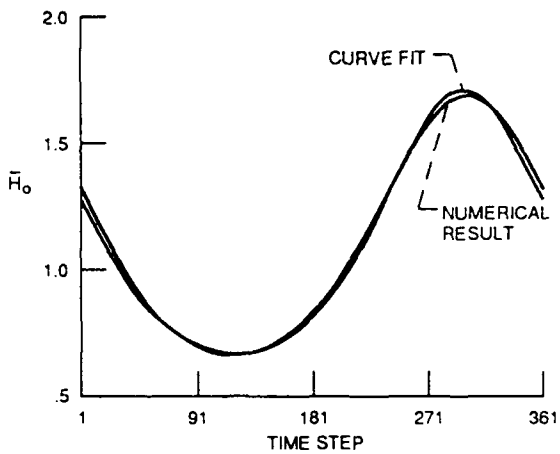

Figure 16. - Comparison of the numerical results with curve fit for $\gamma = 100$.

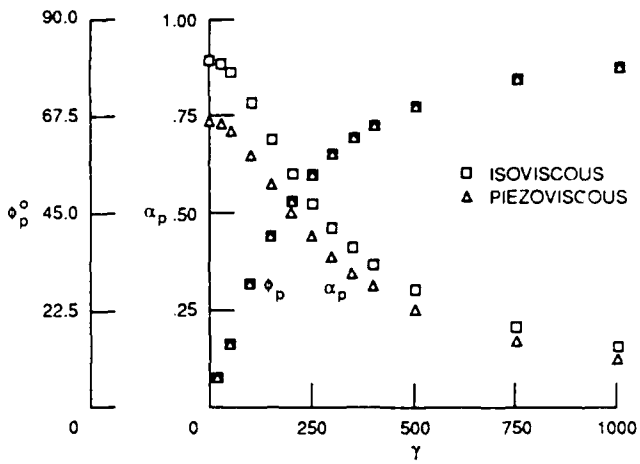

Figure 17. - α_p and ϕ_p in eq. [38] as function of γ.

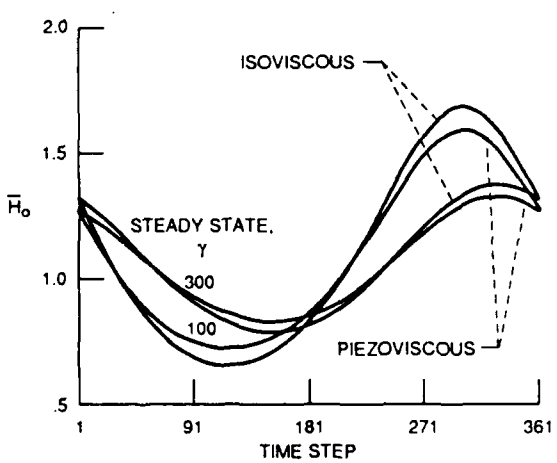

Figure 18. - The comparison of the normalized minimum film thickness distribution between the isoviscous and the piezoviscous solution.

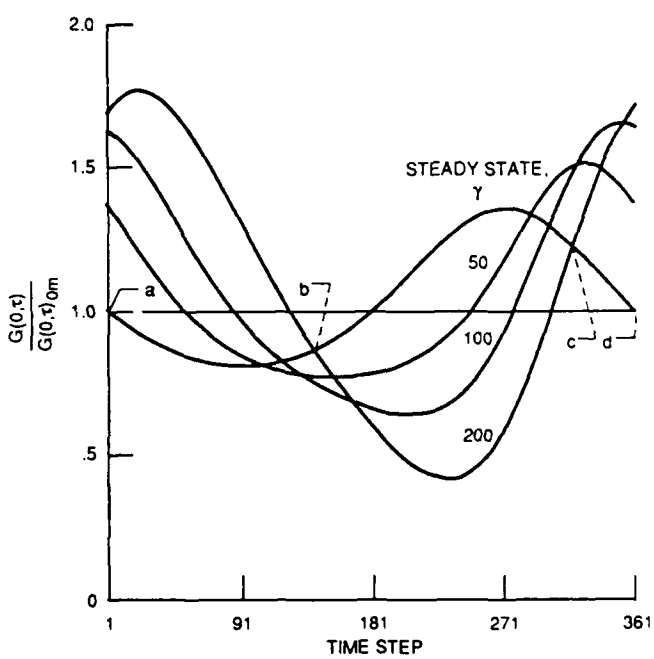

Figure 19. - The distribution of the normalized cavitation boundary at Y = 0 divided by that for the mean load.

NASA
National Aeronautics and Space Administration

Report Documentation Page

1. Report No.	2. Government Accession No.	3. Recipient's Catalog No.
NASA TM-102427 AVSCOM TR 89-C-021		

4. Title and Subtitle

On the Numerical Solution of the Dynamically Loaded Hydrodynamic Lubrication of the Point Contact Problem

5. Report Date

February 1990

6. Performing Organization Code

7. Author(s)

Sang G. Lim, David E. Brewe, and Joseph M. Prahl

8. Performing Organization Report No.

E-5193

9. Performing Organization Name and Address

NASA Lewis Research Center
Cleveland, Ohio 44135-3191
and
Propulsion Directorate
U.S. Army Aviation Research and Technology Activity—AVSCOM
Cleveland, Ohio 44135-3127

10. Work Unit No.

505-63-1A
1L161102AH45

11. Contract or Grant No.

12. Sponsoring Agency Name and Address

National Aeronautics and Space Administration
Washington, D.C. 20546-0001
and
U.S. Army Aviation Systems Command
St. Louis, Mo. 63120-1798

13. Type of Report and Period Covered

Technical Memorandum

14. Sponsoring Agency Code

15. Supplementary Notes

Portions of this material were presented at the Annual Meeting of the Society of Tribologists and Lubrication Engineers, Denver, Colorado, May 7-11, 1990. Sang G. Lim, Dept. of Mechanical Engineering, Case Western Reserve University, Cleveland, Ohio 44106 and NASA Resident Research Associate at Lewis Research Center; David E. Brewe, Propulsion Directorate, U.S. Army Aviation Research and Technology Activity—AVSCOM; Joseph M. Prahl, Dept. of Mechanical Engineering, Case Western Reserve University.

16. Abstract

The transient analysis of hydrodynamic lubrication of a point-contact is presented. A body-fitted coordinate system is introduced to transform the physical domain to a rectangular computational domain, enabling the use of the Newton-Raphson method for determining pressures and locating the cavitation boundary, where the Reynolds boundary condition is specified. In order to obtain the transient solution, an explicit Euler method is used to effect a time march. The transient dynamic load is a sinusoidal function of time with frequency, fractional loading, and mean load as parameters. Results include the variation of the minimum film thickness and phase-lag with time as functions of excitation frequency. The results are compared with the analytic solution to the transient step bearing problem with the same dynamic loading function. The similarities of the results suggest an approximate model of the point contact minimum film thickness solution.

17. Key Words (Suggested by Author(s))	18. Distribution Statement
Hydrodynamic; Lubrication; Transient Analysis; Dynamic; Point contact; Dynamic load; Damping; Periodic load.	Unclassified – Unlimited Subject Category 34

19. Security Classif. (of this report)	20. Security Classif. (of this page)	21. No. of pages	22. Price*
Unclassified	Unclassified	30	A03

NASA FORM 1626 OCT 86

*For sale by the National Technical Information Service, Springfield, Virginia 22161